Translational Oncology
www.transonc.com

Volume 2 Number 3 September 2009 pp. 184–190 184

A Feasibility Study of Parametric Response Map Analysis of Diffusion-Weighted Magnetic Resonance Imaging Scans of Head and Neck Cancer Patients for Providing Early Detection of Therapeutic Efficacy[1]

Craig J. Galbán, Suresh K. Mukherji, Thomas L. Chenevert, Charles R. Meyer, Daniel A. Hamstra, Peyton H. Bland, Timothy D. Johnson, Bradford A. Moffat, Alnawaz Rehemtulla, Avraham Eisbruch and Brian D. Ross

The University of Michigan Medical School, Ann Arbor, MI, USA

Abstract

The parametric response map (PRM) was evaluated as an early surrogate biomarker for monitoring treatment-induced tissue alterations in patients with head and neck squamous cell carcinoma (HNSCC). Diffusion-weighted magnetic resonance imaging (DW-MRI) was performed on 15 patients with HNSCC at baseline and 3 weeks after treatment initiation of a nonsurgical organ preservation therapy (NSOPT) using concurrent radiation and chemotherapy. PRM was applied on serial apparent diffusion coefficient (ADC) maps that were spatially aligned using a deformable image registration algorithm to measure the tumor volume exhibiting significant changes in ADC (PRM_{ADC}). Pretherapy and midtherapy ADC maps, quantified from the DWIs, were analyzed by monitoring the percent change in whole-tumor mean ADC and the PRM metric. The prognostic values of percentage change in tumor volume and mean ADC and PRM_{ADC} as a treatment response biomarker were assessed by correlating with tumor control at 6 months. Pixel-wise differences as part of PRM_{ADC} analysis revealed regions where water mobility increased. Analysis of the tumor ADC histograms also showed increases in mean ADC as early as 3 weeks into therapy in patients with a favorable outcome. Nevertheless, the percentage change in mean ADC was found to not correlate with tumor control at 6 months. In contrast, significant differences in PRM_{ADC} and percentage change in tumor volume were observed between patients with pathologically different outcomes. Observations from this study have found that diffusion MRI, when assessed by PRM_{ADC}, has the potential to provide both prognostic and spatial information during NSOPT of head and neck cancer.

Translational Oncology (2009) 2, 184–190

Introduction

Head and neck squamous cell carcinoma (HNSCC) accounts for 2.5% of all patients whose conditions were newly diagnosed with cancer [1]. Patients whose conditions were diagnosed with locoregional disease have a 5-year relative survival rate of less than 60% [1]. In addition to the poor prognosis, the quality of life of the patient may be affected from overexposure of sensitive areas to radiotherapy. To date, nonsurgical organ preservation therapy (NSOPT) is the standard of care resulting in preservation of the functionality (e.g., swallowing and speech) in the patient while maintaining the same survival rate.

Medical imaging has proven beneficial in diagnosing the conditions of patients with HNSCC [2–8], but little improvement has been made on using these image modalities for monitoring early treatment response. Diffusion magnetic resonance imaging (MRI) has been used for identifying malignancy [3, 5, 9–12] as well as determining late recurrences [13]. Recent work by Kim et al. [14] has shown the utility of diffusion MRI as a surrogate biomarker for early treatment response in HNSCC patients. In that study, changes in whole-tumor mean apparent

Address all correspondence to: Avraham Eisbruch, The Department of Radiation Oncology, The University of Michigan Medical Center, 1500 E Medical Center Dr, Ann Arbor, MI 48109-5010. E-mail: eisbruch@med.umich.edu or Brian D. Ross, The Center for Molecular Imaging, Biomedical Sciences Research Building, 109 Zina Pitcher Pl, Ann Arbor, MI 48109-2200. E-mail: bdross@umich.edu

[1]This study was supported by National Institutes of Health grants P50CA093990, P01CA059827, and P01CA085878.
Received 2 July 2009; Revised 2 July 2009; Accepted 6 July 2009

DOI 10.1593/tlo.09175

diffusion coefficient (ADC), a metric of random thermal motion, of water from pretherapy to 1 week into chemoradiotherapy was shown to correlate with clinical or pathologic assessment of disease. The rise in ADC within complete responders (CRs) after therapy suggested a loss of cell density, which has been observed in previous studies [15,16].

Recently, a voxel-wise approach to evaluate ADC changes was developed [17] and validated [18–20] as an early biomarker for quantifying the spatially heterogeneous response of tumors to therapy. This approach uses registered baseline and early-treatment ADC maps to calculate regional response that may be more sensitive to cellular changes than measurements of the mean change in ADC. This voxel-wise analysis in its most general form is termed the parametric response map (PRM [21]; previously referred to as the functional diffusion map [17]). In a cohort of patients with malignant brain tumors, early diffusion analysis 3 weeks into therapy using PRM_{ADC} was prognostic for later radiographic response [18], time to progression, and overall survival [19], whereas percentage change in mean ADC had failed to demonstrate any predictive value of survival.

We report on the use of diffusion-weighted magnetic resonance imaging (DW-MRI) and PRM analysis in 15 patients with HNSCC treated with NSOPT. The mean ADC at 3 weeks after treatment initiation was found to significantly increase in CRs unlike in partial responders (PRs) where negligible changes were observed. Nevertheless, the percentage change in mean ADC was not found to be significant between PRs and CRs. In contrast, regions of significantly increasing ADC, as assessed by PRM, were found to be significantly larger in CRs than in PRs.

Materials and Methods

Patients

A total of 23 patients were enrolled on an institutional review board–approved prospective trial. Eight patients cannot be evaluated because of claustrophobia [2], metal implants [2], withdrew from study [3], and technical difficulties in diffusion scan [1], leaving 15 patients (Table 1). All patients had AJCC stage III/IV disease and, based on the recommendation of a multidisciplinary head and neck tumor board, were to receive primary treatment with concurrent chemotherapy and radiation. Radiation therapy (RT) was delivered according to standard institutional practice with three-dimensional conformal treatment or intensity-modulated RT with 70 Gy delivered to the gross tumor volumes (nodal or primary), 60 to 63 Gy to high-risk nodal volumes, and 50 to 59.4 Gy delivered to low-risk nodal volumes. At the time of analysis, 2 patients had died of progressive disease, whereas 13 were still alive.

Informed consent was obtained from all patients who were serially imaged approximately 1 week before and approximately 3 weeks after the start of treatment. Tumor response was determined by computed tomography and/or MRI 2 weeks from the end of RT. In addition, a total of six patients had some form of surgical intervention (neck dissection or biopsy) after the completion of RT because of clinical practice or concern for residual mass. Scoring all patients as clinically progressive was done so after tissue confirmation of progression and/or metastatic disease. Patients were stratified by clinical outcome 6 months from the start of treatment into those with (PR, $n = 3$) or without (CR, $n = 12$) progression.

Magnetic Resonance Imaging

All MRI scans were acquired on a 3-T Philips Achieva MRI system (Best, the Netherlands) using an eight-channel head and neck phased-array coil. A head and neck protocol which included a fat-suppressed turbo spin-echo T_2-weighted sequence (field of view [FOV], 240 × 192 mm; matrix, 320 × 256; slice thickness, 4 mm; slices, 30; repetition time/echo time [TR/TE], 5000:120 milliseconds; echo train length [ETL], 15), a non–contrast-enhanced and a gadolinium–diethylenetriamine pentaacetic acid (Gd-DTPA; Bayer HealthCare Pharmaceuticals, Wayne, NJ)–enhanced three-dimensional fast field echo T_1-weighted sequence (FOV, 240 × 240 mm; matrix, 240 × 240; slice thickness, 1 mm; slices, 160; TR/TE/inversion time [TI], 9.9:4.6:1040 milliseconds; turbo factor of 200 echoes), and a DW, single-shot, spin-echo, echo-planar imaging (EPI) series (FOV, 270 × 270 mm; matrix, 205 × 205; slice thickness, 4 mm; slices, 24; TR/TE, 2789:59 milliseconds; *b* factor, 0 and 800 sec/mm^2) with diffusion sensitization along three orthogonal directions. All images were acquired with a SENSitivity Encoding (SENSE) acquisition scheme [22]. The SENSE factor for all images was 2, except the diffusion scans that had a SENSE factor of 3.9. The total duration of this acquisition protocol (including patient setup) was approximately 35 to 60 minutes, with the DW images (DWIs) contributing approximately 2 minutes of scan time.

The product of the three orthogonal DWIs exhibits strong sensitivity to diffusion but without sensitivity to the structural directionality of the tissues. This isotropic feature was crucial for following serial changes in

Table 1. Clinical Characteristics.

Number	Location of Primary	Stage	Chemotherapy	Further Surgery	Disease Status at 6 Months
1	Right tonsil	IVB (T4 N2b)	Cis-5FU	Yes	NED
2	Left base of tongue	IVB (T3 N3)	Carbo-Taxol	Yes	NED
3	Left soft palate	IVB (T2 N3)	Carbo-Taxol	No	Local and regional progression
4	Left tonsil	III (T1 N2a)	Carbo-Taxol	No	NED
5	Left tonsil	IVB (T4 N2c)	Cis-5FU	No	NED
6	Right tonsil	IVB (T2 N3)	Cisplatin	Yes	Regional progression
7	Left tonsil	IVB (T4 N2)	Carbo-Taxol	Yes	Local and regional progression
8	Left base of tongue	IVB (T2 N3)	Carbo-Taxol	No	NED
9	Left base of tongue	III (T3 N0)	Carbo-Taxol	No	NED
10	Unknown primary	III (TX N2a)	Cisplatin	No	NED
11	Left nasopharynx	III (T2 N2)	Cisplatin	No	NED
12	Left pyriform sinus	III (T1 N2b)	Carbo-Taxol	Yes	NED
13	Left tonsil	III (T2 N2b)	Carbo-Taxol	Yes	NED
14	Left tonsil	III (T2 N2b)	Carbo-Taxol	No	NED*
15	Left tonsil	III (T2 N2b)	Carbo-Taxol	No	NED

*Patient with late local and metastatic progression.
NED indicates no evidence of disease.

water diffusion without confounding effects due to tissue orientation. ADC maps were calculated from the DWIs as follows:

$$\mathrm{ADC} = \ln\left[\frac{S_{b_0}}{S_{b_1}}\right] / (b_1 - b_0) \quad (1)$$

where S is the DWI at b values of $b_0 = 0$ and $b_1 = 800$ sec/mm^2.

Subsequent to image registration, contours were manually drawn over tumors as delineated on T_2-weighted, T_1-weighted or contrast-enhanced images by two independent radiologists or radiation oncologist (S.K.M., A.E., or D.A.H., respectively). From the volume-of-interest (VOI) tumor volume and mean ADC were assessed before and 3 weeks after treatment initiation.

Image Registration

Subsequent to contouring the tumors, a geometric warping interpolant, that is, thin-plate spline, algorithm was used to map (warp) the tumor volumes from interval examinations onto the tumor volumes from pretherapy b_0 DWIs (reference data set). Registration was based on the optimization of mutual information between two image data sets and implemented through the use of control points. User input was required for selecting the initial three control points, with additional points performed automatically, in the midtherapy data set that correspond to locations within the VOI of the reference data set. Susceptibility artifacts and patient motion during scanning resulted in misalignment of DWIs to VOIs contoured on anatomic images. Realignment was performed by first warping the b_0 DWIs to the T_1-weighted contrast-enhanced data sets at the pretherapy time point. Subsequent registration of interval examinations were warped to the VOI of the pretherapy b_0 DWIs. As a result of the deformable registration, all serial tumor volumes, as determined by the contours, encompassed the same three-dimensional space as the pretherapy tumor volume. Therefore, only the pretherapy contour was required for performing PRM. All registration was performed using MIAMI-Fuse, which is an in-house image registration software developed by our group [23].

Parametric Response Map

The PRM of ADC (PRM_{ADC}) was determined by first calculating the difference between the ADC values (ΔADC = midtreatment ADC – pretreatment ADC) for each voxel within the tumor pretreatment and at 3 weeks after treatment initiation. Voxels yielding ΔADC greater than a predetermined threshold set to 25 ADC units ($\times 10^{-5}$ mm^2/sec; details described below) were designated as significantly increased and were encoded in red (i.e., $\Delta\mathrm{ADC} > 25 \times 10^{-5}$ mm^2/sec). Blue voxels represent volumes whose ADC values significantly decreased by more than 25×10^{-5} mm^2/sec (i.e., $\Delta\mathrm{ADC} < -25 \times 10^{-5}$ mm^2/sec) and the green voxels within the tumor represent unchanged ADC values (i.e., absolute value of ΔADC was $\leq 25 \times 10^{-5}$ mm^2/sec). The volume fractions within the tumor as determined by PRM_{ADC} were denoted by PRM_{ADC+} (increased ADC), PRM_{ADC-} (decreased ADC), and PRM_{ADC0} (unchanged ADC). PRM thresholds of significant change were empirically assessed over a range of ΔADCs (0-70), and the optimal threshold was determined from a receiver operating characteristic (ROC) curve analysis of PRM_{ADC+} and PRM_{ADC-} for predicting tumor control at 6 months from the end of treatment. PRM_{ADC+} with a threshold of ±25 ADC units provided the best correlation with tumor control.

Statistical Analysis

A paired 2-tailed Student's t test was used for comparison of baseline tumor volume and mean ADC with 3-week midtreatment values. In addition, differences in tumor volume and mean ADC, at individual time points, were assessed between patients with clinically progressive and nonprogressive disease and between primary and lymph node tumor lesions by an unpaired 2-tailed Student's t test. Group comparisons were also performed for percentage change in tumor volume and mean ADC and PRM_{ADC}. The correlation of the representative imaging parameters with tumor control at 6 months after treatment initiation was assessed by an ROC curve analysis. All statistical computations were performed with a statistical software package (SPSS; SPSS, Inc, Chicago, IL), and results were declared statistically significant at $P < .05$.

Results

Clinical Data

A total of 15 patients were evaluated, and at the time of analysis, 2 patients had died of progressive disease while 13 were still alive. Eleven of these had no evidence of recurrence and two had recurrence (one with nodal recurrence and one with both local and metastatic progressions; Table 1). Because of N2 or N3 lymph nodes, a total of three patients (Table 1: nos. 1, 2, and 6) underwent planned surgical dissection of regional lymph nodes after the completion of RT; therefore, these nodal volumes could not be included for later radiographic evaluation because they were surgically resected before the 12-week time point.

Representative Patients

Figure 1 displays unregistered pretreatment (*top row*) and 3 weeks after treatment initiation (*bottom row*) MR images along with corresponding ADC histograms from the whole-tumor volume for a patient with a HNSCC of the left base of the tongue. Enlarged right cervical lymph nodes, denoted within the *yellow dashed region*, are readily evident as hyperintense lesions on T_2-weighted and contrast-enhanced images (Figure 1, *A* and *C*) and as hypointense lesions on T_1-weighted images (Figure 1*B*). The pathologically enlarged lymph nodes are also apparent on the ADC maps (Figure 1*D*) with values shown to be inversely correlated with cellular density [24] greater than the adjacent muscle. The corresponding pretreatment diffusion histogram reflects a broad ADC distribution with some areas exhibiting a very low ADC consistent with high cellularity with a mean ADC of 120×10^{-5} mm^2/sec. At 3 weeks after treatment initiation, the nodal tumor volume had increased by 2.6%, whereas a 27.5% rise in mean tumor ADC to 153×10^{-5} mm^2/sec was observed. Given the large nodal disease and minimal volumetric response, this patient underwent a clinically necessitated cervical lymph node dissection that revealed no evidence of residual disease (CR) and was alive and free of disease 35 months from the completion of treatment.

Figure 2 displays unregistered before (*top row*) and 3 weeks after treatment initiation images (*bottom row*) along with corresponding ADC histograms from the whole-tumor volume for a patient treated for HNSCC of the right tonsil. Enlarged lymph nodes were found to be hypointense on T_1-weighted images and hyperintense on T_2-weighted images and were determined to enhance in the presence of a contrast agent on T_1-weighted images. A mean tumor ADC of 117×10^{-5} mm^2/sec was measured before treatment, which increased by 17.9% to 138×10^{-5} mm^2/sec at 3 weeks after treatment initiation. At the 3-week time point, nodal volumes were found to be 11% smaller. Subsequently, this patient underwent a salvage neck dissection, and despite a greater shrinkage in tumor, there were residual viable tumor cells identified in

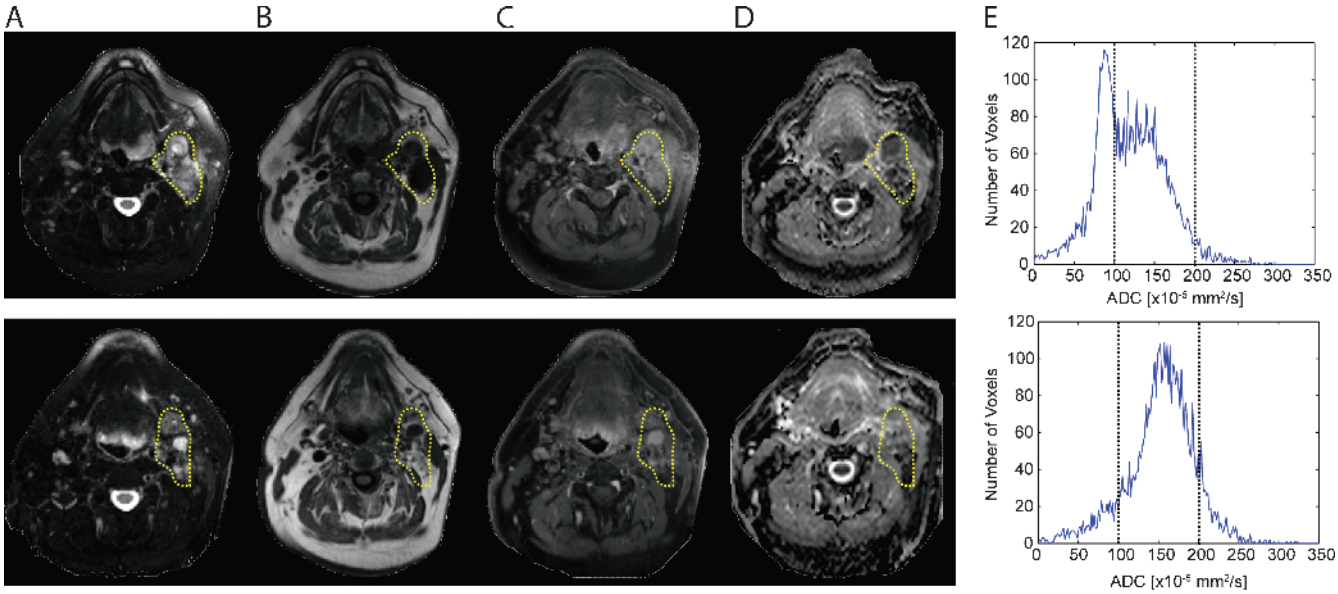

Figure 1. Unregistered before (top row) and 3 weeks after treatment initiation (bottom row): (A) T_2-weighted, (B) T_1-weighted, (C) contrast-enhanced T_1-weighted images, and (D) ADC maps with corresponding (E) ADC histograms from the whole tumor of a patient treated for HNSCC of the left base of the tongue. The tumor is outlined by the yellow contour line. This patient was subsequently determined to be a CR to therapy.

the nodal dissection. The clinical outcome of this patient was PR, and the patient was free of disease at 16 months after salvage surgery.

Whole-Tumor Analysis of Volume and ADC

A total of 26 lesions, 12 primary tumors and 14 lymph node volumes, were analyzed to determine whether differences in whole-tumor mean ADC values were evident between primary and lymph node tumors before and 3 weeks after treatment induction. No significant difference in mean ADC was observed between primary tumor and the nodal masses at baseline or 3 weeks after treatment initiation (Table 2). At the 3-week interval, mean ADC values of lymph nodes significantly increased from baseline values ($P < .0001$) with significant observable tumor shrinkage found in both primary ($P = .005$) and lymph node ($P < .0001$) tumors. Although not significant, primary lesions revealed a trend of increased mean ADC after treatment ($P = .06$). Because primary and lymph node tumors' responses to treatment were similar, primary lesions and nodal masses were pooled for correlation of ADC changes with patient outcome information.

Between clinical groups, no significant tumor volumetric differences were observed at the 3-week posttreatment induction time interval. In

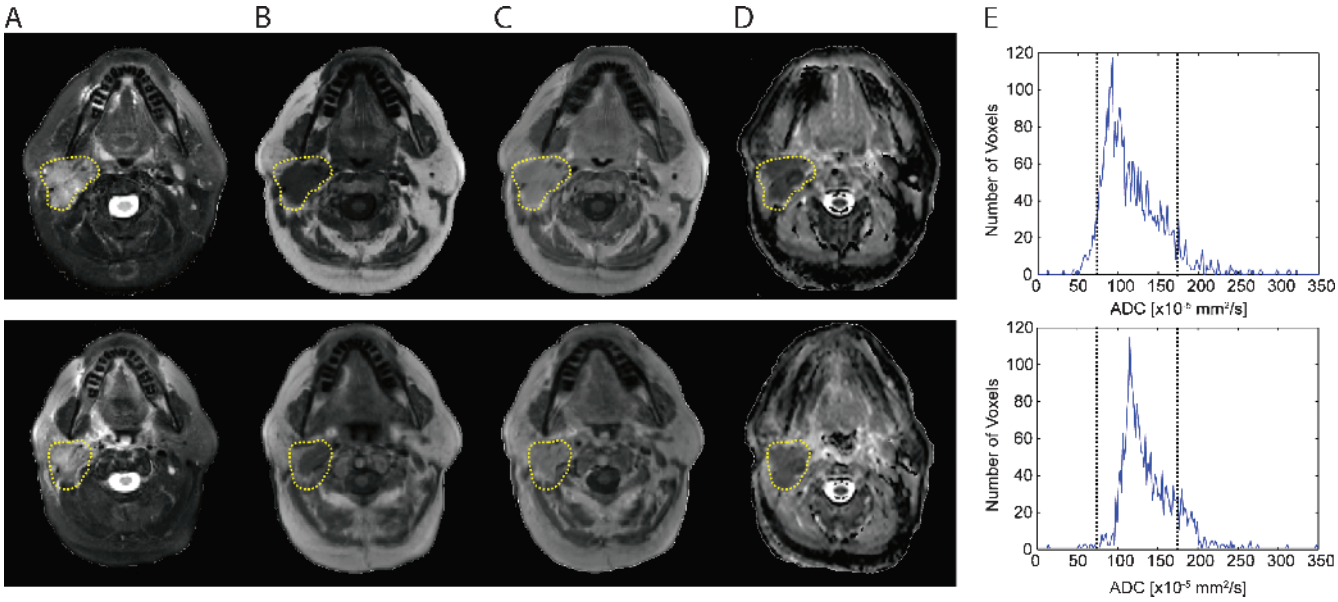

Figure 2. Unregistered before (top row) and 3 weeks after treatment initiation (bottom row): (A) T_2-weighted, (B) T_1-weighted, (C) contrast-enhanced T_1-weighted images, and (D) ADC maps with corresponding (E) ADC histograms from the whole tumor from a patient treated for HNSCC of the right tonsil. The tumor is encompassed within the yellow contour. The clinical outcome of this patient was a PR.

contrast, tumor volumes in both patient groups were found to significantly decrease from baseline values at 3 weeks after treatment initiation. However, before and after treatment, no significant differences were observed in tumor mean ADC when stratified by clinical outcome (Table 2). Nevertheless, patients diagnosed as CRs demonstrated a significant rise in midtreatment whole-tumor mean ADC value from baseline values ($P < .0001$), whereas PRs demonstrated negligible changes in mean ADC values at 3 weeks after treatment induction.

Parametric Response Mapping of ADC (PRM_{ADC})

Results from PRM_{ADC} analysis of the two patients (Figures 1 and 2) are shown in Figure 3. More than 63% of the tumor volume was found to have a significant increase in ADC (depicted as *red voxels*), suggesting massive cell kill in the tumor mass, for the patient (Figure 1) who exhibited a complete response to therapy (Figure 3*A*). Regions within the tumor volume, approximately 9%, were found to have a significant drop in ADC (depicted as *blue voxels*). This patient was later found to have no evidence of malignancy after salvage neck dissection. In comparison, the patient found to be a PR (salvage neck dissection was positive for residual cancer) was found to have less of the tumor volume responding to therapy than the previous patient (Figure 3*A*), with 46% of the tumor volume producing a significant increase in ADC (Figure 3*B*). A small fraction of the tumor was found to have a significant decrease in ADC (PRM_{ADC-} = 6%).

In Figure 4*A*, the percentage changes in tumor volume and percentage of tumor with significantly increased ADC values as assessed by the metric PRM_{ADC+} were significantly associated with disease control at 6 months ($P < .05$). Tumor volume had decreased by up to 43 ± 6% in CRs, whereas tumors from PRs dropped by only 22 ± 4%. When the groups were assessed by PRM_{ADC}, PRM_{ADC+} was found to be composed of 55 ± 4% of the tumor volume in CRs, with PRs only showing 37 ± 7% of the tumor volume responding to treatment. In contrast, negligible differences in percentage change in mean ADC (Figure 4*A*) and PRM_{ADC-} (data not shown) were observed between clinical groups. Further evaluation of the predictive value of these methods was performed using an ROC curve analysis correlated with clinical progression at 6 months (Figure 4*B*). The percentage changes in tumor volume and whole-tumor mean ADC were not significantly associated with clinical progression (area under the curve [AUC] = 0.758, $P = .06$ and AUC = 0.758, $P = .06$; respectively), whereas PRM_{ADC+} (AUC = 0.825, $P = .02$) was predictive of clinical progression at 6 months. PRM_{ADC-} did not provide a significant prognostic measure of response.

Discussion

Recently, we demonstrated in an animal model of HNSCC treated with chemoradiotherapy that a greater rise in tumor ADC early into treatment predicted tumor control and animal survival [25], suggesting that the magnitude of early change in tumor ADC values may be a sensitive early measure of tumor response. As previously reported, the quantification of changes in diffusion MRI scans during and after cytotoxic therapies has shown that these changes precede tumor regression in both animal models and human tumors [18–20,24,26–28]. Therefore, ADC values as assessed by PRM were quantified to determine whether tumor response could be identified within the first 3 weeks of RT in patients with HNSCC when there would still be time to adapt treatment based on an early imaging biomarker readout if it predicted insufficient response to treatment.

In all cases, ADC histogram distributions were heterogeneous and typically skewed (Figures 1 and 2). These broad ADC distributions are consistent with the known heterogeneous morphology of malignant head and neck tumors as previously reported [3, 4, 12]. After 3 weeks of treatment, the distribution of ADC values generally shifted to a higher value, which correlated with a net increase in mean ADC values for these tumors (Figures 1 and 2). Furthermore, the increase in mean ADC values was found to be lower in those patients with later progression of disease than patients without evidence of residual disease (Figure 4*A*). The overall heterogeneity of tumor response can attenuate the prognostic value of the histogram-based metric of change in mean tumor ADC values, which could account for a loss in its sensitivity to differentiate CRs from PRs. Unlike histogram-based whole-tumor ADC measurements, PRM can circumvent the added complexity of tumor heterogeneity by accounting for the full anatomic and spatial information of the DW-MR images. Regional changes in ADC values within the tumor were observed in the PRM color overlays (Figure 3, *A* and *B*).

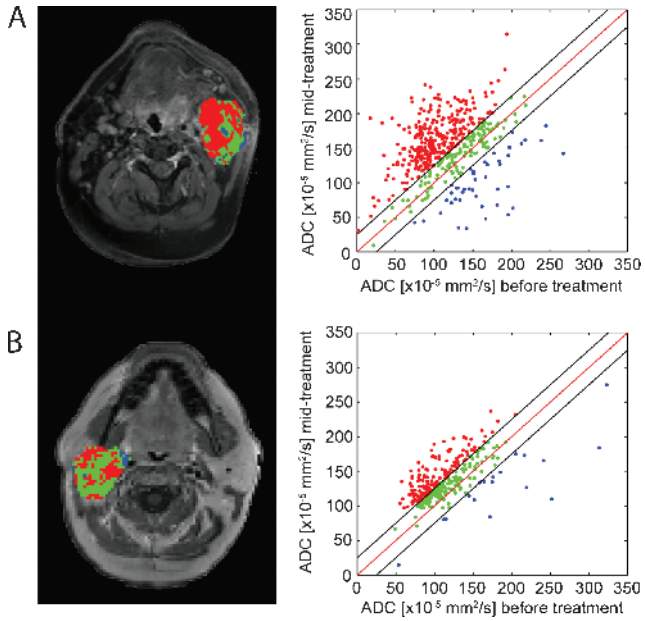

Figure 3. Representative slices of PRM_{ADC} for patients whose conditions were diagnosed as (A) CR and (B) PR; color-coded VOIs are overlaid on contrast-enhanced T_1-weighted MR images before therapy and corresponding scatter plots for quantification and distribution of ADC before and 3 weeks after treatment initiation for the entire tumor volume. Unity and threshold designating significant change in ADC within the scatter plot are presented by red and black lines, respectively. Voxels with significant increased, decreased, or unchanged ADC values were assigned as red, blue, and green, respectively.

Table 2. Early Response of Volume and Tumor ADC Values at 3 Weeks after Treatment Initiation.

	Volume [cm^3] (SEM)		ADC [$\times 10^{-5}$ mm^2/sec] (SEM)	
	Pretreatment	Midtreatment	Pretreatment	Midtreatment
Primary	**28.8 (9.5)**	**19.3 (7.2)**	145.8 (11.3)	163.3 (10.6)
Lymph nodes	**43.7 (9.9)**	**29.6 (10.2)**	**122.5 (5.0)**	**153.4 (5.1)**
CR	**30.6 (5.9)**	**18.2 (5.4)**	**133.5 (7.7)**	**162.9 (6.3)**
PR	**57.8 (22.3)**	**47.1 (19.7)**	132.7 (8.6)	141.5 (9.5)

Clinical outcome is presented as CR and PR. Bolded values indicate significant differences between pretreatment and midtreatment values as determined by paired Student's *t* test ($P < .05$). Statistical differences in tumor volume or ADC were not observed between tumor type and clinical outcome at pretreatment or midtreatment time points.

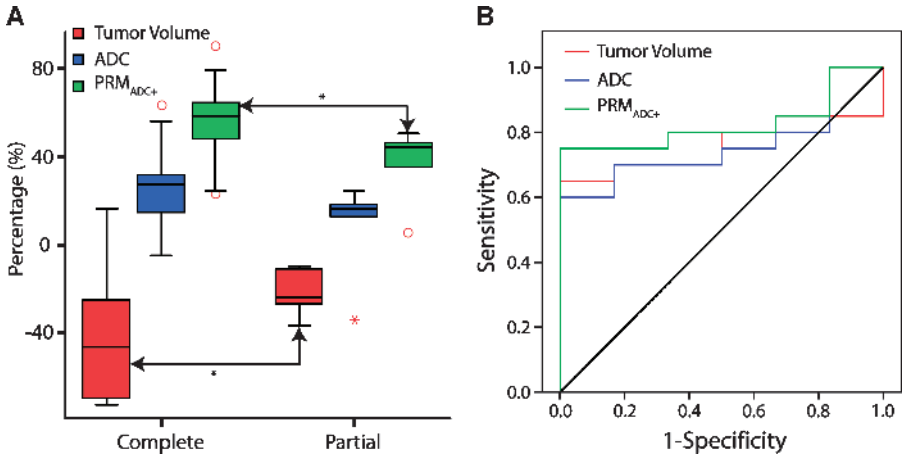

Figure 4. Box plot (A) and receiver operating characteristic curve (B) of response metrics: percentage change in tumor volume (red) and mean ADC values (blue) and PRM analysis representing the percentage of the tumor volume, which exhibited a significant increase in ADC (red; PRM_{ADC+}). *Significant differences between outcome groups as assessed by an unpaired Student's *t* test with $P < .05$.

The volume of tumor with a significant rise in diffusion (PRM_{ADC+}; *red voxels*) was directly correlated with favorable clinical outcome, which is similar to that observed in patients with primary brain tumors treated with RT where the PRM_{ADC+} (presented as V_I) was directly correlated with patient survival [19]. In the current study, there was no association between the volume of tumor with decreasing ADC (PRM_{ADC-}; *blue voxels*) and clinical progression, which also confirms the results obtained in brain tumor patients [19]. Thus, in this patient population, we found that analysis of ADC maps by PRM was more sensitive to small differences in response than whole-tumor metrics.

Application of PRM in patients with HNSCC requires additional image after the processing steps not required when applied to brain tumor patient data. The rapid imaging techniques used for acquiring DWIs, which uses EPI, suffer from susceptible artifacts at air-tissue interfaces. This susceptibility results in distortion of the images. Even sequences carefully optimized will suffer from some image distortion in the DWI at moderate *b* values (≥800 sec/mm^2). Fat located in the extracranial head and neck poses additional difficulties in acquiring DWI data sets. The signal from fat is especially problematic in DWI. For one, the fat signal resonates at a slightly different frequency from water, which may result in a shift in the fat signal from its true anatomic location. To make matters worse, fat has a very slow diffusivity (0.05×10^{-3} mm^2/sec), which, if near the tumor, may cause an underestimation of the true ADC. Finally, motion artifacts, which are very common in patients with advanced-stage head and neck cancer often with salivary stasis and difficulty breathing, introduce difficulties in aligning images acquired even during the same scanning session. All of these imaging artifacts pose hardships when applying image fusion. Unlike rigid-body registration, which is used on serial image data sets from glioma patients, nonlinear image fusion algorithms are required to register DWIs to anatomic or serial DWI data sets.

The limitations of the current study include the relatively small number of patients and the single time point evaluated to measure changes in diffusion. Of 15 patients, only 3 were found to have progressive disease 6 months after treatment. To offset these small numbers, multiple tumors in a patient were treated independently resulting in 26 individual samples. This approach was deemed to be valid as response outcomes were assessed individually by tumor pathology for each tumor and not for the patient as a whole. Optimization of PRM sensitivity for the quantification of early treatment response in patients with HNSCC may be improved by using a different time interval. In fact, preclinical models have shown that the greatest ability for diffusion MRI to predict response was before a significant change in tumor volume had occurred [17,24,29]. Therefore, given the significant tumor regression observed after 2 to 3 weeks of treatment, the maximal PRM response may have occurred earlier than the measurement interval evaluated in this present study. A similar phenomenon was observed in patients treated with neoadjuvant chemoradiotherapy for rectal cancer where DWI at 1 week identified a group of patients with a rise in ADC who later had favorable pathologic features (necrosis and negative surgical margins), whereas diffusion assessment at 1 month demonstrated an overall decline in diffusion, which was not prognostic and which the authors attributed to fibrosis [30,31]. In addition, investigators at the University of Pennsylvania recently obtained encouraging results with diffusion MRI as early as 1 week into a course of chemoradiotherapy for head and neck cancer with minimal volume changes [14]. As a note, all of these studies used the percentage change in mean ADC as their outcome metric. Here, we observed no predictive value in mean ADC, whereas PRM_{ADC} had produced significant results between pathologically distinct groups. Because of the differences observed between the recent report of Kim et al. [14] and the present results, further investigation of the efficacy of mean ADC and PRM_{ADC} with a larger cohort of patients and studied over multiple time points is warranted. This would provide for an opportunity to optimize the timing of the DW-MRI interval examination, thus potentially improving the sensitivity of the PRM imaging biomarker metric.

A significant result of this present study was the determination that it was feasible to perform high-order registration (warping) on DWI head and neck lesions using interval examinations. Imaging of the head and neck with EPI can be problematic because of image distortion resulting from susceptibility at air-tissue interfaces [4]. Even while acquiring data using parallel imaging technique, such as SENSE, image distortion can render full-affine registration algorithms ineffective for fusing serial images. We found that higher-order registration techniques were required for the implementation of PRM. Because inaccurate registration of serial maps would randomize the PRM metrics resulting in a lack of correlation with clinical outcomes, the fact that PRM analysis was determined to statistically correlate to the clinical progression supports the accuracy of the registration technique used in this study.

In summary, to date, NSOPT is the standard of care for patients whose conditions were diagnosed with HNSCC, resulting in the preservation of functionality (e.g., swallowing and speech) in the patient while maintaining the current survival rate. Diffusion MRI provides voxel-wise information on tumor status after chemoradiotherapy. Tumor lesions in serial MR images were registered into a single geometric frame using a deformable image registration algorithm. This was a key step for implementing the PRM, which is a voxel-wise technique for quantifying therapeutic-induced changes. Diffusion measurements as assessed by PRM_{ADC}, and not percentage change of the mean diffusion, at 3 weeks into a course of chemoradiotherapy were found to be predictive of disease control at 6 months in patients. The change in the ADC, as measured by DW-MRI and assessed by PRM, may serve as a potential imaging biomarker for quantifying early therapeutic efficacy in patients with HNSCC that can be readily incorporated into a clinical head and neck cancer treatment protocol. DW-MRI, when assessed by PRM, has the potential to provide prognostic and spatial information during NSOPT of head and neck cancer. In this study, significant treatment-induced increases in tumor ADC values were detectable and spatially resolved using PRM analysis. The results of this study provide the foundation and rationale for pursuing a larger trial to determine more fully the potential of PRM analysis for DW-MRI data as an early biomarker for monitoring therapeutic efficacy in patients with head and neck cancer. On validation in a larger study, PRM may aid in the individualization of head and neck cancer treatment regimens.

References

[1] Jemal A, Siegel R, Ward E, Hao Y, Xu J, Murray T, and Thun MJ (2008). Cancer statistics, 2008. *CA Cancer J Clin* **58**, 71–96.

[2] Lemort M, Canizares AC, and Kampouridis S (2006). Advances in imaging head and neck tumours. *Curr Opin Oncol* **18**, 234–239.

[3] Srinivasan A, Dvorak R, Perni K, Rohrer S, and Mukherji SK (2008). Differentiation of benign and malignant pathology in the head and neck using 3T apparent diffusion coefficient values: early experience. *AJNR Am J Neuroradiol* **29**, 40–44.

[4] Srinivasan A, Dvorak R, Rohrer S, and Mukherji SK (2008). Initial experience of 3-tesla apparent diffusion coefficient values in characterizing squamous cell carcinomas of the head and neck. *Acta Radiol* **49**, 1079–1084.

[5] Cho H, Ackerstaff E, Carlin S, Lupu ME, Wang Y, Rizwan A, O'Donoghue J, Ling CC, Humm JL, Zanzonico PB, et al. (2009). Noninvasive multimodality imaging of the tumor microenvironment: registered dynamic magnetic resonance imaging and positron emission tomography studies of a preclinical tumor model of tumor hypoxia. *Neoplasia* **11** (3), 247–259, 2p following 259.

[6] Harisinghani M, Ross RW, Guimaraes AR, and Weissleder R (2007). Utility of a new bolus-injectable nanoparticle for clinical cancer staging. *Neoplasia* **9** (12), 1160–1165.

[7] Witney TH, Kettunen MI, Day SE, Hu DE, Neves AA, Gallagher FA, Fulton SM, and Brindle KM (2009). A comparison between radiolabeled fluorodeoxyglucose uptake and hyperpolarized (13)C-labeled pyruvate utilization as methods for detecting tumor response to treatment. *Neoplasia* **11** (6), 574–582, 1p following 582.

[8] Young MR, Ileva LV, Bernardo M, Riffle LA, Jones YL, Kim YS, Colburn NH, and Choyke PL (2009). Monitoring of tumor promotion and progression in a mouse model of inflammation-induced colon cancer with magnetic resonance colonography. *Neoplasia* **11** (3), 237–246, 1p following 246.

[9] Lee KC, Bradley DA, Hussain M, Meyer CR, Chenevert TL, Jacobson JA, Johnson TD, Galban CJ, Rehemtulla A, Pienta KJ, et al. (2009). A feasibility study evaluating the functional diffusion map as a predictive imaging biomarker for detection of treatment response in a patient with metastatic prostate cancer to the bone. *Neoplasia* **9** (12), 1003–1011.

[10] Padhani AR, Liu G, Koh DM, Chenevert TL, Thoeny HC, Takahara T, Dzik-Jurasz A, Ross BD, Van Cauteren M, Collins D, et al. (2009). Diffusion-weighted magnetic resonance imaging as a cancer biomarker: consensus and recommendations. *Neoplasia* **11** (2), 102–125.

[11] Seierstad T, Folkvord S, Roe K, Flatmark K, Skretting A, and Olsen DR (2007). Early changes in apparent diffusion coefficient predict the quantitative antitumoral activity of capecitabine, oxaliplatin, and irradiation in HT29 xenografts in athymic nude mice. *Neoplasia* **9** (5), 392–400.

[12] Wang J, Takashima S, Takayama F, Kawakami S, Saito A, Matsushita T, Momose M, and Ishiyama T (2001). Head and neck lesions: characterization with diffusion-weighted echo-planar MR imaging. *Radiology* **220**, 621–630.

[13] Vandecaveye V, De Keyzer F, Nuyts S, Deraedt K, Dirix P, Hamaekers P, Vander Poorten V, Delaere P, and Hermans R (2007). Detection of head and neck squamous cell carcinoma with diffusion weighted MRI after (chemo)radiotherapy: correlation between radiologic and histopathologic findings. *Int J Radiat Oncol Biol Phys* **67**, 960–971.

[14] Kim S, Loevner L, Quon H, Sherman E, Weinstein G, Kilger A, and Poptani H (2009). Diffusion-weighted magnetic resonance imaging for predicting and detecting early response to chemoradiation therapy of squamous cell carcinomas of the head and neck. *Clin Cancer Res* **15**, 986–994.

[15] Szafer A, Zhong J, Anderson AW, and Gore JC (1995). Diffusion-weighted imaging in tissues: theoretical models. *NMR Biomed* **8**, 289–296.

[16] Chenevert TL, McKeever PE, and Ross BD (1997). Monitoring early response of experimental brain tumors to therapy using diffusion magnetic resonance imaging. *Clin Cancer Res* **3**, 1457–1466.

[17] Moffat BA, Chenevert TL, Lawrence TS, Meyer CR, Johnson TD, Dong Q, Tsien C, Mukherji S, Quint DJ, Gebarski SS, et al. (2005). Functional diffusion map: a noninvasive MRI biomarker for early stratification of clinical brain tumor response. *Proc Natl Acad Sci USA* **102**, 5524–5529.

[18] Hamstra DA, Chenevert TL, Moffat BA, Johnson TD, Meyer CR, Mukherji SK, Quint DJ, Gebarski SS, Fan X, Tsien CI, et al. (2005). Evaluation of the functional diffusion map as an early biomarker of time-to-progression and overall survival in high-grade glioma. *Proc Natl Acad Sci USA* **102**, 16759–16764.

[19] Hamstra DA, Galban CJ, Meyer CR, Johnson TD, Sundgren PC, Tsien C, Lawrence TS, Junck L, Ross DJ, Rehemtulla A, et al. (2008). Functional diffusion map as an early imaging biomarker for high-grade glioma: correlation with conventional radiologic response and overall survival. *J Clin Oncol* **26**, 3387–3394.

[20] Moffat BA, Chenevert TL, Meyer CR, McKeever PE, Hall DE, Hoff BA, Johnson TD, Rehemtulla A, and Ross BD (2006). The functional diffusion map: an imaging biomarker for the early prediction of cancer treatment outcome. *Neoplasia* **8**, 259–267.

[21] Galban CJ, Chenevert TL, Meyer CR, Tsien C, Lawrence TS, Hamstra DA, Junck L, Sundgren PC, Johnson TD, Ross DJ, et al. (2009). The parametric response map is an imaging biomarker for early cancer treatment outcome. *Nat Med* **15**, 572–576.

[22] Pruessmann KP, Weiger M, Scheidegger MB, and Boesiger P (1999). SENSE: sensitivity encoding for fast MRI. *Magn Reson Med* **42**, 952–962.

[23] Meyer CR, Boes JL, Kim B, Bland PH, Zasadny KR, Kison PV, Koral K, Frey KA, and Wahl RL (1997). Demonstration of accuracy and clinical versatility of mutual information for automatic multimodality image fusion using affine and thin-plate spline warped geometric deformations. *Med Image Anal* **1**, 195–206.

[24] Chenevert TL, Stegman LD, Taylor JM, Robertson PL, Greenberg HS, Rehemtulla A, and Ross BD (2000). Diffusion magnetic resonance imaging: an early surrogate marker of therapeutic efficacy in brain tumors. *J Natl Cancer Inst* **92**, 2029–2036.

[25] Hamstra DA, Lee KC, Moffat BA, Chenevert TL, Rehemtulla A, and Ross BD (2008). Diffusion magnetic resonance imaging: an imaging treatment response biomarker to chemoradiotherapy in a mouse model of squamous cell cancer of the head and neck. *Transl Oncol* **1**, 187–194.

[26] Mardor Y, Pfeffer R, Spiegelmann R, Roth Y, Maier SE, Nissim O, Berger R, Glicksman A, Baram J, Orenstein A, et al. (2003). Early detection of response to radiation therapy in patients with brain malignancies using conventional and high *b*-value diffusion-weighted magnetic resonance imaging. *J Clin Oncol* **21**, 1094–1100.

[27] Theilmann RJ, Borders R, Trouard TP, Xia G, Outwater E, Ranger-Moore J, Gillies RJ, and Stopeck A (2004). Changes in water mobility measured by diffusion MRI predict response of metastatic breast cancer to chemotherapy. *Neoplasia* **6**, 831–837.

[28] Hamstra DA, Rehemtulla A, and Ross BD (2007). Diffusion magnetic resonance imaging: a biomarker for treatment response in oncology. *J Clin Oncol* **25**, 4104–4109.

[29] Hamstra DA, Lee KC, Tychewicz JM, Schepkin VD, Moffat BA, Chen M, Dornfeld KJ, Lawrence TS, Chenevert TL, Ross BD, et al. (2004). The use of ^{19}F spectroscopy and diffusion-weighted MRI to evaluate differences in gene-dependent enzyme prodrug therapies. *Mol Ther* **10**, 916–928.

[30] DeVries AF, Kremser C, Hein PA, Griebel J, Krezcy A, Ofner D, Pfeiffer KP, Lukas P, and Judmaier W (2003). Tumor microcirculation and diffusion predict therapy outcome for primary rectal carcinoma. *Int J Radiat Oncol Biol Phys* **56**, 958–965.

[31] Kremser C, Judmaier W, Hein P, Griebel J, Lukas P, and de Vries A (2003). Preliminary results on the influence of chemoradiation on apparent diffusion coefficients of primary rectal carcinoma measured by magnetic resonance imaging. *Strahlenther Onkol* **179**, 641–649.